Theoretical and experimental analysis of a base-excited rotor

Nicolas Driot, Claude-Henri Lamarque, Alain Berlioz

▶ **To cite this version:**

Nicolas Driot, Claude-Henri Lamarque, Alain Berlioz. Theoretical and experimental analysis of a base-excited rotor. Journal of Computational and Nonlinear Dynamics, 2006, 1 (3), pp.257-263. 10.1115/1.2209648 . hal-00814612

HAL Id: hal-00814612
https://hal.science/hal-00814612v1

Submitted on 18 Oct 2024

HAL is a multi-disciplinary open access archive for the deposit and dissemination of scientific research documents, whether they are published or not. The documents may come from teaching and research institutions in France or abroad, or from public or private research centers.

L'archive ouverte pluridisciplinaire **HAL**, est destinée au dépôt et à la diffusion de documents scientifiques de niveau recherche, publiés ou non, émanant des établissements d'enseignement et de recherche français ou étrangers, des laboratoires publics ou privés.

Distributed under a Creative Commons Attribution - NonCommercial 4.0 International License

Accepted Manuscript

Theoretical and Experimental Analysis of a Base-Excited Rotor

N. Driot[1]
Laboratoire de Dynamique des Machines et des Structures UMR CNRS 5006, INSA LYON, Villeurbanne, France

C. H. Lamarque
Laboratoire Géo-Matériaux URA CNRS 1652, ENTPE LYON, Vaulx-en-Velin, France

A. Berlioz
Laboratoire de Génie Mécanique de Toulouse EA 814, Universite Paul Sabatier, Toulouse, France

In this study, the dynamic behavior of a flexible rotor system subjected to support exci-tation (imposed displacements of its base) is analyzed. The effect of an excitation on lateral displacements is investigated from theoretical and experimental points of view. The study focuses on behavior in bending. A mathematical model with two gyroscopic and parametrical coupled equations is derived using the Rayleigh-Ritz method. The the-oretical study is based on both the multiple scales method and the normal form approach. An experimental setup is then developed to observe the dynamic behavior permitting the measurement of lateral displacements when the system's support is subjected to a sinu-soidal rotation. The experimental results are favorably compared with the analytical and numerical results.

1 Introduction

Many industrial applications contain rotor dynamic systems. They have been extensively studied in the case of fixed bases (meaning fixed supports) and nowadays the dynamic behavior of such rotors is well established [1]. However, in systems such as rotors of aircraft engines during maneuvers of the aircraft or power plant reactor rotors at the time of seismic activity, the whole system may be subjected to many sudden imposed displacements. This leads to the appearance of parametric terms in the equations of motion. As a consequence, an imposed displacement of supports could drastically change the behavior of the rotor with the system being subjected to parametric instabilities. The number of works dealing with this specific area of investigation is quite low. The response of such a rotor support subjected to white noise excitation was studied using the modal approach developed by Subbiah et al. [2]. In [3], the effect of base flexibility was taken into account in a rotor modeled by additional stiffness matrices and the effects on Campbell diagram were pointed out. A theoretical model with six base excitation components was proposed by Suarez et al., [4] in the case of seismic excitation. Likewise, Beley-Sayettat proposed a general study in [5]. In two papers, Ganessan and Sankar studied the dynamic behavior of a rotor and pointed out the complex phenomena observed by using a multiple scales approach, as well as giving a good explanation of the parametric effects [6,7]. Kang et al. studied the influence of the foundation on natural frequencies using finite elements and substructuring techniques [8]. Some other works concern the experimental investigations of rotors whose support are subjected to motion; see Edwards et al., [9]. A theoretical approach using an impedance technique was used by Bonello and Brennan [10]. Recent works have been related to a shock study [11]. The work presented herein focuses on the particular behavior of a rotor under a base rotational motion. This special base excitation exhibits typical dynamical behaviors as the one observed for parametrically excited system. The completeness of this work is achieved by first, building a theoretical realistic modeling of this phenomenon and second, by conducting some dynamical measurements. Concerning the theoretical part, the dynamical responses are found by time integration scheme and normal form analysis. The latter is well suited to analyze quasi-periodic responses.

The present paper is organized as follows: the theoretical model is presented in Sec. 2 in which a numerical and experimental stability analysis is also conducted. The setup and its main characteristics are described in the Sec. 3, after which some general experimental dynamical data are presented using non-typical running conditions. Particular running conditions are investigated in Sec. 4. Then, the modeling is used to compare the predicted dynamic behaviors with that observed in the setup. The last section is devoted to the conclusions.

2 Theoretical Model

2.1 Equations of Motion. The investigated rotor is shown in Fig. 1(*a*), and the frames used are illustrated in Fig. 1(*b*). The equations of motion [12] are developed from the Rayleigh-Ritz method and the derivation of equations is briefly described in Appendix A. The dynamic modeling of this rotor does not include the exciter and the stinger. Indeed, their respective compliances are far away from those of the test rotor. In what follows, the base excitation is equal to an angular velocity excitation, i.e., rotation around axis x_s, [$X=0$, $Y=0$, $Z=0$, $\alpha=\gamma=0$ and $\beta=a\sin(\omega t)$] expressed in frame R_0 (see Appendix B and Fig. 1). The equations are time dependent (parametric excitation due to time dependent stiffnesses) and can be strongly nonlinear, depending on the motion of the rotor base. In what follows, they are:

$$m\ddot{q}_1 - \Omega I_{y2}\dot{q}_2 + [k - \omega^2 A\cos^2(\omega t)]q_1 = \Omega\omega B\cos(\omega t)$$

$$m\ddot{q}_2 + \Omega I_{y2}\dot{q}_1 + [k - \omega^2 C\cos^2(\omega t)]q_2 = \omega^2 D\sin(\omega t) \qquad (1)$$

In the system of Eq. (1), m is the modal mass (first bending mode shape) of the rotor, k is the modal stiffness of the rotor (the bearings are identical), and I_{y2} the inertia of the disk. Ω and ω are the rotational speed of the rotor and the frequency of the base excitation of the imposed displacement, respectively. Components A, B, C, and D of the forcing terms are related to the mechanical characteristics of the rotor (see Appendix B). To simplify the task, the system of Eq. (1) can be rewritten as

[1]Corresponding author.

Accepted Manuscript

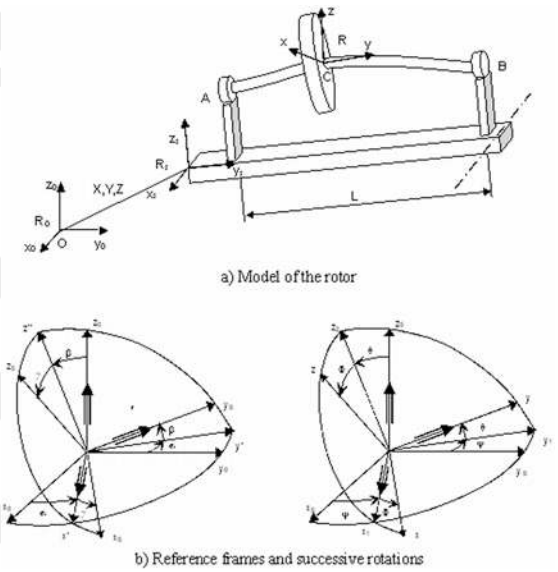

Fig. 1 Description of the rotor

$$\ddot{q}_1 + \lambda_1 \dot{q}_2 + [\alpha - f_{11}\cos^2(\omega t)]q_1 = f_{12}\cos(\omega t)$$
$$\ddot{q}_2 - \lambda_1 \dot{q}_1 + [\alpha - f_{21}\cos^2(\omega t)]q_2 = f_{22}\sin(\omega t) \quad (2)$$

with the following substitutions:

$$f_{11} = \frac{A\omega^2}{m}, \quad f_{12} = \frac{B\omega\Omega}{m}, \quad f_{21} = \frac{C\omega^2}{m}, \quad f_{22} = \frac{D\omega^2}{m},$$
$$\text{and} \quad \lambda_1 = -\Omega I_{y2} \quad (3)$$

As observed in the first runs, the experimental rotor setup exhibited a residual unbalanced response. Thus the unbalance is then defined as a mass m_u located on disk at a short distance d from the geometric center of the shaft. In order to compare the numerical results to the experimental ones, a special forcing term is added in the right-hand side of Eq. (2). Moreover, the amplitudes of the dynamic responses reveal the existence of a damping factor. This issue is taken into account by introducing an equivalent viscous damping factor ξ in both Eq. (2). The system of equations is now rewritten as

$$\ddot{q}_1 + \lambda_1 \dot{q}_2 + \xi \dot{q}_1 + [\alpha - f_{11}\cos^2(\omega t)]q_1 = f_{12}\cos(\omega t) + f_{13}\sin(\Omega t)$$
$$\ddot{q}_2 - \lambda_1 \dot{q}_1 + \xi \dot{q}_2 + [\alpha - f_{21}\cos^2(\omega t)]q_2 = f_{22}\sin(\omega t) + f_{23}\cos(\Omega t) \quad (4)$$

with

$$f_{13} = \frac{M_u}{m} \quad \text{and} \quad f_{23} = \frac{M_u}{m}, \quad \text{and} \quad M_u = m_u d \quad (5)$$

The system of Eq. (4) is more realistic than the system of Eq. (1).

2.2 Stability Analysis. System of Eq. (4) includes parametric terms $q_i \cos^2(\omega t)$, which can generate instabilities. The stability is studied using the multiple scales method with a development up to the first order (see Appendix B). For this task, the right-hand side of Eq. (4) is set to zero and the damping is not considered as it is well known that the worst cases of instability appear when damping is zero [14].

It is important to point out that large parametric terms lead to nonsymmetrical rotor behavior. The natural frequencies had to be computed considering the time-averaged Eq. (4). Consequently, the natural frequencies of the rotor at rest are slightly different.

This asymmetry at rest is completely controlled by the term $(a\omega)^2$. Furthermore, the natural frequencies are also dependent on the value of ω. Finally, the computed two first natural ($\cong$29 Hz and $\cong$35 Hz) frequencies are of same order of magnitude as those found in Sec. 3.2. These higher values reveal that the bearing stiffnesses used are slightly too high.

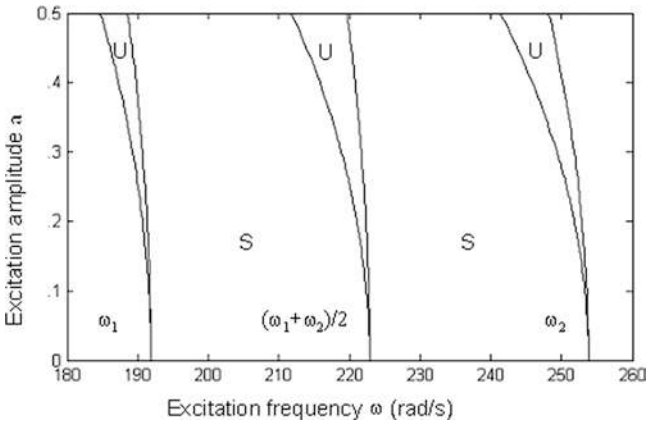

Fig. 2 Transition curves between stability and instability areas

Without going into further detail, the external resonances are obtained using the procedure described in [13]. The different possibilities are related to the values of the natural frequencies of the Campbell diagram, ω_1 and ω_2, respectively,

$$\omega \approx \omega_1; \quad \omega \approx \omega_2; \quad \omega \approx \frac{(\omega_1 + \omega_2)}{2}; \quad \omega \approx \frac{(\omega_2 - \omega_1)}{2} \quad (6)$$

The instability zones are shown in Fig. 2. In fact, only the first three cases will be considered next; the last case is less interesting because of the low frequency it implies.

2.3 Normal Forms Analysis. The application of the method of normal forms to previous is not directly suitable. Let the system of Eq. (4) be transformed with the following equality:

$$q_1(t) = Q_1(t) + f(t)$$
$$q_2(t) = Q_2(t) + g(t) \quad (7)$$

The time functions $f(t)$ and $g(t)$ are functions of class C^l defined as the solutions of the following linear of Eq. (8):

$$\ddot{f} + \lambda_1 \dot{g} + \xi \dot{f} + \alpha f = f_{12}\cos(\omega t) + f_{13}\sin(\Omega t)$$
$$\ddot{g} - \lambda_1 \dot{f} + \xi \dot{g} + \alpha g = f_{22}\sin(\omega t) + f_{23}\cos(\Omega t) \quad (8)$$

Since the system of Eq. (8) consists of two linear coupled differential equations of second order, $f(t)$ and $g(t)$ are obtained easily. Their spectra exhibit two harmonic components located at Ω and ω.

The new system of Eq. (9) for variables Q_1 and Q_2 is obtained after substituting the equality (7) in (4) and using differential equations (8)

$$\ddot{Q}_1 + \lambda_1 \dot{Q}_2 + \xi \dot{Q}_1 + [\alpha - f_{11}\cos^2(\omega t)]Q_1 = f_{11}\cos^2(\omega t) f(t)$$
$$\ddot{Q}_2 - \lambda_1 \dot{Q}_1 + \xi \dot{Q}_2 + [\alpha - f_{21}\cos^2(\omega t)]Q_2 = f_{21}\cos^2(\omega t) g(t) \quad (9)$$

The system of Eq. (9) is now rewritten as a system in complex valued form containing only differential equations of the first order with third-degree polynomial nonlinearities. Then, the method of normal forms is applied. The method provides a truncated uniform expansion of variables Q_1 and Q_2 by using near identity transformations in the terms of normal coordinates. In our case, truncation is achieved at order three at least. Consequently, the resonant terms are found to be of order three with a small magnitude. Thus, Q_1 and Q_2 are functions of time whose spectra mainly

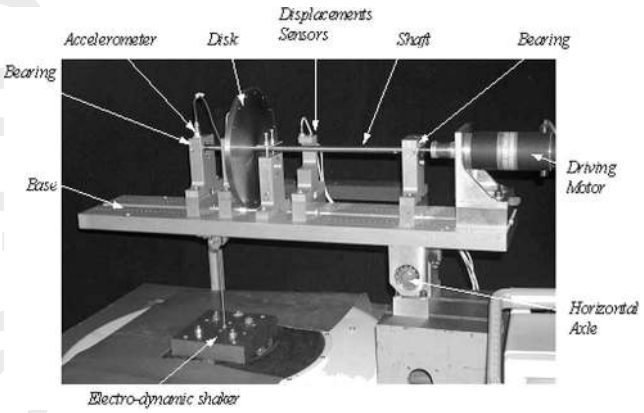

Fig. 3 Experimental setup for a base excitation around the horizontal direction

contain components located at Ω and ω. The numerical results are now compared to the experimental results for particular running conditions, i.e., $\omega = n\Omega$ with n being successively an integer or a rational number.

3 Experiments on the Excited Rotor Support

3.1 Description of the Experimental Setup. The investigated rotor is shown in Fig. 1(a), and the frames used are illustrated in Fig. 1(b). The rotor is driven by a servomotor and consists of a flexible shaft with a rigid disk supported by two bearings. These bearings are strictly identical. We assume that there is no bearing anisotropy. The mass of the rotor is equal to $m_r = 1.53$ kg. The rotation speed is controlled through a feedback system. The responses of the vertical and horizontal displacements of the shaft were measured on planes parallel to the shaft's cross section. Contactless sensors are located close to the middle of the shaft.

An electrodynamic shaker (Gearing & Watson 4700N) was used to apply the base excitation matching the imposed displacement. The base excitation is considered to be sinusoidal imposed rotation around the horizontal axis x_s (Fig. 1)

$$\dot{\alpha}_s = a\omega \cos(\omega t) \tag{10}$$

The head of the shaker was linked to the base via a connecting push-rod. The shaker was powered by a power control unit (G&W DS4) and a function generator (HP33120A). The displacement of the head of the shaker was monitored by an accelerometer and held constant in the frequency range of interest. During testing, all the measurements were stored and displayed on a real-time digital scope. Balancing was done using a classical procedure for 1600, 1800, and 2000 rpm. The aim is to obtain an acceptable value of the displacement (lower than 0.5 mm) at the first critical speed. This balancing is achieved on a single plane, and the influence coefficients method was used to find the unbalance to be added. As a consequence, the residual unbalancing was found to be equal to $M_u = 2.5 \times 10^{-4}$ kg m and is located on the disk. The two first natural frequencies (ω_i $i = 1, 2$) of the rotor, both at rest and in rotation, were obtained with a classical impulse (low-amplitude) response by measuring the power density spectra of the displacement responses. These natural frequencies are measured when the rotor is subjected to its support excitation. As a consequence, they may be different to those obtained for the same rotor without support excitation. A similar test was used at rest to measure the damping factor ξ. The validations of the numerical simulations were based on the experimental data obtained with the rotor setup shown in Fig. 3.

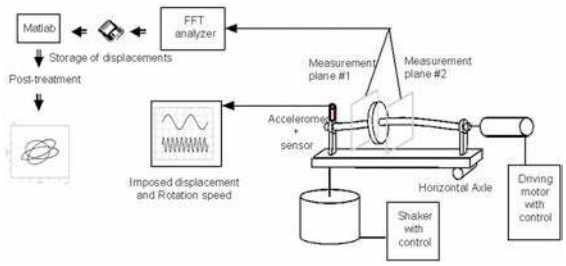

Fig. 4 Block diagram of the experimental setup

The digital data recording system is shown schematically in Fig. 4. Lastly, the main characteristics of the setup are presented in Table. 1.

3.2 Experimental Results for General Running Conditions. The three parameters that define the experimental running conditions are: a, the amplitude of the base excitation; ω, the frequency of the base excitation; and Ω, the rotor frequency. We first consider the case of general running conditions, that is to say when ω and Ω are not linked by any mathematical relationship. The amplitude of the angular deviation due to the base excitation is chosen such that the angular deviation is close to 2 deg/s. The dynamic displacement responses are measured at the middle of the shaft in x direction (q_1 variable) and z direction (q_2 variable).

Figure 5(a) displays the phase plane obtained when the running conditions are: $\Omega = 40$ Hz, $\omega = 55$ Hz, and $a = 2 \times 10^{-5}$. The shape of the orbits seems to be a torus. According to these running conditions, the two first natural frequencies of the rotor were close to $\omega_1 \approx 28$ Hz and $\omega_2 \approx 34$ Hz. These natural frequencies are those of the first bending mode in x and z directions, respectively. They are respectively named as the backward and forward modes. The first critical speed is found to be close to 2250 rpm. Such ordinary orbits are difficult to observe as the phase plane does not appear to be fixed. Figure 5(b) displays the phase plane provided by a numerical computation (seventh-eighth-order Runge-Kutta) when running conditions are the previous ones. In a qualitative point of view, the agreement between the two results is quite good. Indeed, the orders of magnitude are identical and both phase planes reveal a quasi-periodic solution. The relative differences between results could be explained by the fact that the residual unbalance is not necessary in phase with the base excitation.

The dynamical responses are quasi-periodic functions. As rotational frequency Ω is low, the three-dimensional (3D) bending deformed shape of the rotor is a simple combination of two one-dimensional (1D) first bending deformed shape of a supported-supported beam in the x and z directions. On the contrary, each shape vibrates at a different frequency, revealing quasi-periodic behaviors.

Table 1 Main characteristics of the setup

Length of the shaft (m)	$L = 0.4$
Radius of the shaft (m)	$R_1 = 5 \times 10^{-3}$
Radius of the disk (m)	$R_2 = 0.1$
Thickness of the disk (m)	$h = 1 \times 10^{-2}$
Young modulus (Pa)	$E = 2.05 \times 10^{11}$
Mass per unit volume (kg/m^3)	$\rho = 7800$
Rotation speed range (rpm)	Ω, 0 to 4000
Residual unbalance (kg m)	$M_u = 2.5 \times 10^{-4}$
Damping factor	$\xi = 50$/m
Mass of the rotor (kg)	$m_r = 1.534$
Amplitude of angular velocity excitation	$a = 2 \times 10 - 5$

Accepted Manuscript

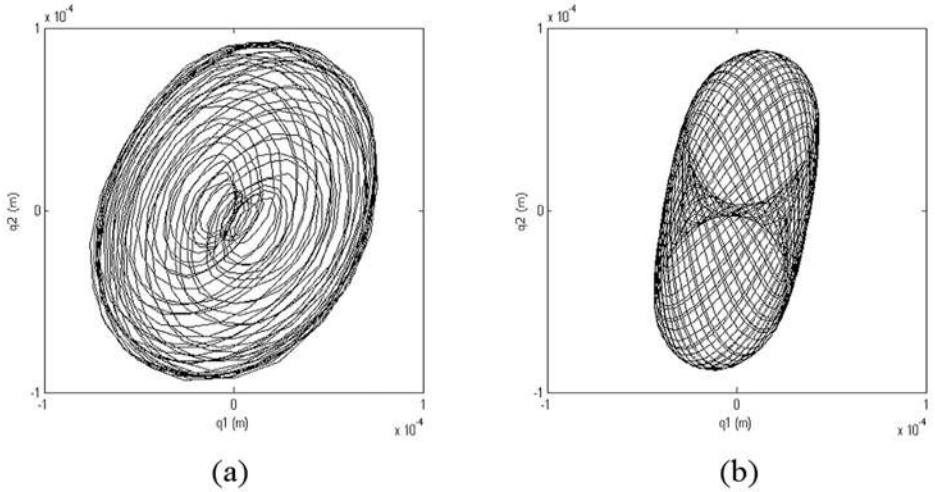

Fig. 5 Experimental orbits when Ω and ω are ordinary: (*a*) experimental and (*b*) numerical

4 Comparisons Between Experimental and Numerical Results

The aim of this section is to compare experimental dynamical responses to numerical ones for given particular running conditions. The analytical data are provided by the method of normal forms neglecting the damping effect. The numerical results correspond to the dynamical responses obtained with a classical time integration scheme, i.e., the seventh-eighth-order continuous Runge-Kutta method. All next figures show displacement $x(q_1)$ of the shaft against the displacement $z(q_2)$ at the middle of the shaft. Lastly, the amplitude of the angular excitation is equal to $a=2\times10^{-5}$.

4.1 Orbits for $\omega=n\Omega$, Integer n. In this particular case, the orbits are "fixed" and match well with periodic solutions. Figure 6 displays the phase plane for $\Omega=20$ Hz and $n=2,3,4,5$.

Numerical and analytical results are in very good agreement with the experimental data, and the shape and magnitude of the orbits are well described by the two numerical methods. As the exciting frequencies are low, the excited deformed shape corresponds to the first modal shape. This shape vibrates mostly at Ω and ω, shifted by a phase. The periodic solutions could be explained by the fact that phases between the two harmonic vibrations vanish after a small number of periods. The dynamical behavior becomes periodic. The amplitudes of the normal coordinates are very small in this case: the normal form method shows that nonlinear effects are actually very small here. This is why only experimental and numerical results are provided in Secs. 4.2 and 4.3.

4.2 Orbits for $\omega=n\Omega$, Rational n. The same phenomenon occurs when n is a rational number rewritten as

$$\omega=\frac{\beta}{\chi}\Omega \tag{11}$$

where β and $\times$ are integers. In this case, the higher $\times$ is, the more complicated the shape of the orbit becomes. Figure 7 shows particular orbits when $\Omega=40$ Hz and $n=1/2$, 2/3, and 3/4. The correlation between experimental and numerical results is very good.

4.3 Orbits When ω is Close to ω_1 or ω_2. It is now interesting to look at the cases where ω is close to one of the resonant frequencies ω_1 and ω_2. These resonant frequencies depend both on the values of ω and Ω. It should be noted that the resonant conditions are difficult to obtain by experiments because of low damping values. Consequently, the primary resonant conditions are never achieved by experiments in this study. In fact, there exist many primary resonant cases ($\Omega\neq0$), some of them can occur simultaneously,

$$\omega_1=\omega \quad \text{or} \quad \omega_1=\Omega$$

$$\omega_2=\omega \quad \text{or} \quad \omega_2=\Omega \tag{12}$$

As the sensitivity of these natural frequencies decreases as ω is low, we next consider that ω_1 and ω_2 are only dependent on Ω. Figure 8 shows particular orbits when $\Omega=20$ Hz and ω is close to

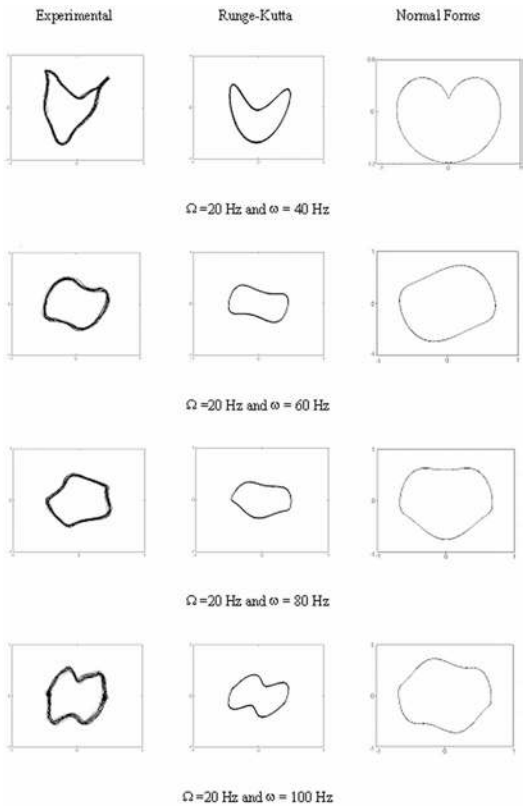

Fig. 6 Particular orbits when $\omega=n\Omega$, n integer (q_1 versus q_2 in 10^{-4} m)

Accepted Manuscript

Accepted Manuscript

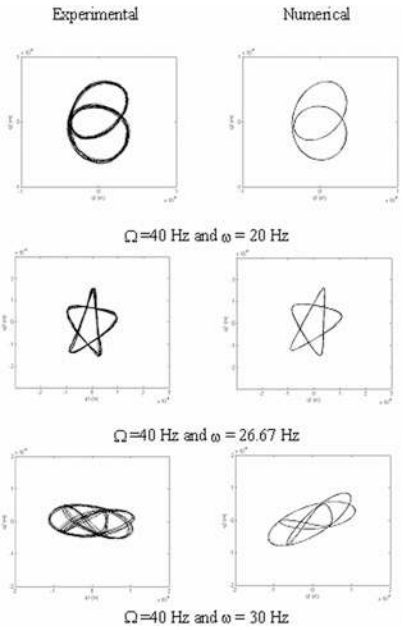

Fig. 7 Particular orbits when $\omega = n\Omega$, n rational

one of the resonant frequencies.

The orbits are fixed because it is still possible to find a rational number as the ratio between ω and Ω. This situation is equivalent to the previous one of Sec. 4.2.

Lastly, Figure 9 shows several orbits obtained when Ω =40 Hz. In all cases, comparison between the experimental and numerical results reveals that the modeling of the setup provides accurate results.

5 Conclusions

This paper outlines several results of measurements and computations on a rotor with a base excitation. A simplified model based on the Rayleigh-Ritz method is used. From these equations, using the method of multiple scales appears that instabilities may exist for specific displacement of the support. The normal form method is used to study the dynamic behavior of the parametrically excited rotor. The comparison between the results obtained with analytical methods, experimental investigations on the setup and a step-by-step computation is quite satisfactory.

By and large, it appears that the normal form method is very suitable for studying this kind of phenomena even though the nonlinearity effect is small. Likewise, the method can be easily applied to a system subjected to large parametric excitations. Further developments will concern a more sophisticated rotor including geometrical nonlinearities and internal damping.

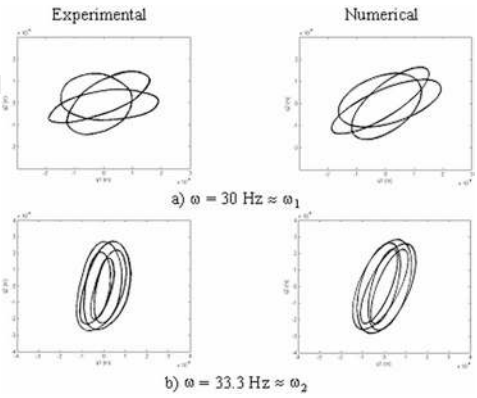

Fig. 8 Particular orbits when Ω=20 Hz

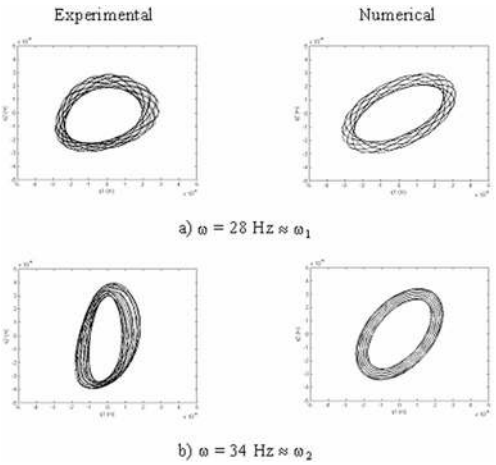

Fig. 9 Particular orbits when Ω=40 Hz

Acknowledgment

This study was financed by the French Ministry of Research and Education. The authors would like to thank Dr. Matthieu Duchemin and Professor Guy Ferraris who provided part of the experimental and numerical data.

Nomenclature

a = amplitude of the support excitation
A, B, C, D = components of the forcing terms
d = distance from the geometric center of the shaft
f_{ij} = reduced components of external forces vector (i=1 to 2, j=1 to 3)
$f(y)$, $g(y)$, $h(y)$ = displacement function first and second partial derivatives
I_{ai}, I_{mi}, I_{yi}, = intermediate constant values (i=1 to 2)
I_x, I_z = area moments of inertia of the shaft
I_{Da}, I_{Dm} = asymmetric and symmetric components of the tensor inertia of the disk
I_a, I_m = asymmetric and symmetric components of the tensor inertia of the shaft
L = length of the shaft
l_1 = location of the center of the disk
M_D = mass of the disk
M_1, M_2, M_5 = intermediate constant values of mass
m_u = mass unbalance
m_{ij}, c_{ij}, k_{ij} = components of mass, gyroscopic and damping matrices
m = components of mass matrix in the case of a base excitation
q_i, Q_i, F_{qi} = generalized independent coordinates and forces
$R_0(x_0, y_0, z_0)$ = fixed initial frame
$R_s(x_s, y_s, z_s)$ = frame fixed to the rotor base
$R(x, y, z)$ = frame fixed to the disk
S = area of the shaft section,
X, Y, Z = Translational motions of the support
$u(y), w(y)$ = displacements along x and z directions

Greek Symbols

$\dot{\alpha}_s, \dot{\beta}_s, \dot{\gamma}_s$ = components of the angular velocity of the support
ξ = viscous damping factor
ψ, θ, ϕ = successive rotations from R to R_s

Ω = constant angular velocity of the rotor
ω_1, ω_2 = natural frequencies of the system
ω = frequency of the external excitation
ρ = mass per unit volume

Appendix A: Derivation of the Equations for the Simplified Model

The basic assumptions for the energies are as follows [12]:

Energy of the disk. The disk, which is located in C at a constant coordinate l_1 from the point A (see Fig. 1(b)), is assumed to be rigid and is characterized by its kinetic energy.

Energy of the shaft. The elementary kinetic energy for a current point of coordinates (a thin shaft section) is seen as a generalization of the case of the disk. Moreover, the motion of the support does not modify the strain energy of the shaft [1].

Mass unbalance. The kinetic energy of the mass unbalance is the kinetic energy of a mass m_u located on the disk at a distance d from the geometric center of the shaft.

The angles ψ and θ (Fig. 1) are considered to be small, the angular velocity of the rotor is considered to be constant, S is the constant cross section of the shaft, ρ is the mass per unit volume, and I_x and I_z are the moments of inertia. The displacement function $f(y)$ chosen for the Rayleigh-Ritz method is the exact first mode shape of a beam assumed to be simply supported at both ends and with a constant cross section in bending (secondary effects are not considered here). Hence, $g(y)$ and $h(y)$ are the first and second derivatives of the displacement function, respectively. For the two lateral modal displacements q_1 and q_2, these assumptions lead to

$$u(y,t) = f(y)q_1(t) = \sin\left(\frac{\pi y}{L}\right)q_1(t)$$
$$w(y,t) = f(y)q_2(t) = \sin\left(\frac{\pi y}{L}\right)q_2(t) \tag{A1}$$

Introducing this displacement function into the kinetic energy of the system [12], Lagrange's equations are applied, leading to the general equations of motion in a compact form

$$\begin{bmatrix} m_{11} & m_{12} \\ m_{21} & m_{22} \end{bmatrix}\begin{bmatrix} \ddot{q}_1 \\ \ddot{q}_2 \end{bmatrix} + \begin{bmatrix} c_{11} & c_{12} \\ c_{21} & c_{22} \end{bmatrix}\begin{bmatrix} \dot{q}_1 \\ \dot{q}_2 \end{bmatrix} + \begin{bmatrix} k_{11} & k_{12} \\ k_{21} & k_{22} \end{bmatrix}\begin{bmatrix} q_1 \\ q_2 \end{bmatrix} = \begin{bmatrix} f_1 \\ f_2 \end{bmatrix} \tag{A2}$$

where the different terms in the matrices depend both on the characteristics of the rotor and on the motion of the rotor support (X, Y, Z are the imposed translational motions of the support and $\dot{\alpha}_s$, $\dot{\beta}_s$, $\dot{\gamma}_s$ are the imposed angular velocities of the support, all expressed in R_0 frame). The general forms are those presented in [12] and are recalled in what follows:

Mass Matrix

$$m_{11} = M_2 + I_{m2} - I_{a2}\cos(2\Omega t)$$
$$m_{22} = M_2 + I_{m2} + I_{a2}\cos(2\Omega t) \tag{A3}$$
$$m_{12} = m_{21} = I_{a2}\sin(2\Omega t)$$

Gyroscopic and Damping Matrix

$$c_{11} = -c_{22} = 2I_{a2}\Omega\sin(2\Omega t)$$
$$c_{12} = \dot{\beta}_S(2M_2 + 2I_{m2} - I_{y2}) - \Omega I_{y2} + 2I_{a2}\Omega\cos(2\Omega t) \tag{A4}$$
$$c_{21} = -\dot{\beta}_S(2M_2 + 2I_{m2} - I_{y2}) + \Omega I_{y2} + 2I_{a2}\Omega\cos(2\Omega t)$$

Stiffness Matrix

$$k_{11} = k + \dot{\alpha}_S^2(I_{m2} - I_{y2}) - \dot{\beta}_S^2(M_2 + I_{m2} - I_{y2}) - \dot{\gamma}_S^2 M_2 + \dot{\beta}_S\Omega I_{y2} + [(\dot{\alpha}_S^2 - \dot{\beta}_S^2 - 2\Omega\dot{\beta}_S)I_{a2} - k_a]\cos(2\Omega t) - (\ddot{\beta}_S + \dot{\alpha}_S\dot{\gamma}_S)I_{a2}\sin(2\Omega t)$$

$$k_{22} = k + \dot{\gamma}_S^2(I_{m2} - I_{y2}) - \dot{\beta}_S^2(M_2 + I_{m2} - I_{y2}) - \dot{\alpha}_S^2 M_2 + \dot{\beta}_S\Omega I_{y2} + [(-\dot{\gamma}_S^2 + \dot{\beta}_S^2 + 2\Omega\dot{\beta}_S)I_{a2} + k_a]\cos(2\Omega t) + (\ddot{\beta}_S - \dot{\alpha}_S\dot{\gamma}_S)I_{a2}\sin(2\Omega t) \tag{A5}$$

$$k_{12} = (\dot{\alpha}_S\dot{\gamma}_S + \ddot{\beta}_S)(M_2 + I_{m2} - I_{y2}) + [(\dot{\beta}_S^2 - \dot{\alpha}_S^2 + 2\Omega\dot{\beta}_S)I_{a2} + k_a]\sin(2\Omega t) - (\ddot{\beta}_S + \dot{\alpha}_S\dot{\gamma}_S)I_{a2}\cos(2\Omega t)$$

$$k_{21} = (\dot{\alpha}_S\dot{\gamma}_S - \ddot{\beta}_S)(M_2 + I_{m2}) - I_{y2}\dot{\alpha}_S\dot{\gamma}_S + [(\dot{\beta}_S^2 - \dot{\alpha}_S^2 + 2\Omega\dot{\beta}_S)I_{a2} + k_a]\sin(2\Omega t) - (\ddot{\beta}_S + \dot{\alpha}_S\dot{\gamma}_S)I_{a2}\cos(2\Omega t)$$

External Forces

$$f_1 = m_u df(l_1)[-(\ddot{\beta}_S + \dot{\alpha}_S\dot{\gamma}_S)\cos(\Omega t) + [(\dot{\beta}_S + \Omega)^2 + \dot{\gamma}_S^2]\sin(\Omega t)] + (M_5 + I_{m1})(\ddot{\gamma}_S - \dot{\alpha}_S\dot{\beta}_S) + I_{y1}\dot{\alpha}_S(\Omega + \dot{\beta}_S) + M_1[\ddot{\gamma}_S(2\dot{Y} + \dot{\gamma}_S X - \dot{\alpha}_S Z) - \dot{\beta}_S(2\dot{Z} + \dot{\alpha}_S Y - \dot{\beta}_S X) - \ddot{X} - \ddot{\beta}_S Z + \ddot{\gamma}_S Y] + I_{a1}[-(\ddot{\gamma}_S + \dot{\alpha}_S\dot{\beta}_S + 2\Omega\dot{\alpha}_S)\cos(2\Omega t) + (-\ddot{\alpha}_S + \dot{\gamma}_S\dot{\beta}_S + 2\Omega r)\sin(2\Omega t)]$$

$$f_2 = m_u df(l_1)[(\ddot{\beta}_S - \dot{\alpha}_S\dot{\gamma}_S)\sin(\Omega t) + ((\dot{\beta}_S + \Omega)^2 + \dot{\alpha}_S^2)\cos(\Omega t)] - (M_5 + I_{m1})(\ddot{\alpha}_S + \dot{\gamma}_S\dot{\beta}_S) + I_{y1}\dot{\gamma}_S(\Omega + \dot{\beta}_S) + M_1[-\dot{\alpha}_S(2\dot{Y} + \dot{\gamma}_S X - \dot{\alpha}_S Z) + \dot{\beta}_S(2\dot{X} + \dot{\beta}_S Z - \dot{\gamma}_S Y) - \ddot{Z} + \ddot{\beta}_S X - \dot{\alpha}_S Y] + I_{a1}[-(\ddot{\alpha}_S + \dot{\gamma}_S\dot{\beta}_S + 2\Omega\dot{\gamma}_S)\cos(2\Omega t) + (\dot{\gamma}_S + \dot{\alpha}_S\dot{\beta}_S + 2\Omega\dot{\alpha}_S)\sin(2\Omega t)] \tag{A6}$$

In order to point out the effect of the mean inertia and asymmetry, the following notation is used:

$$I_{Dm} = \frac{I_{Dx} + I_{Dz}}{2} \quad \text{and} \quad I_{Da} = \frac{I_{Dx} - I_{Dz}}{2} \tag{A7}$$

The following terms are characteristics of the rotor and time dependent:

$$I_{m1} = I_{Dm}g(l_1) + \int_0^L \rho I_m g(y)dy$$
$$I_{a1} = I_{Da}g(l_1) + \int_0^L \rho I_a g(y)dy \tag{A8}$$
$$I_{m2} = I_{Dm}g^2(l_1) + \int_0^L \rho I_m g^2(y)dy$$
$$I_{a2} = I_{Da}g^2(l_1) + \int_0^L \rho I_a g^2(y)dy$$
$$I_{y1} = I_{Dy}g(l_1) + 2\int_0^L \rho I_m g(y)dy \tag{A9}$$
$$I_{y2} = I_{Dy}g^2(l_1) + 2\int_0^L \rho I_m g^2(y)dy$$

Accepted Manuscript

$$M_1 = M_D f(l_1) + \int_0^L \rho S f(y)dy$$

$$M_2 = M_D f^2(l_1) + \int_0^L \rho S f^2(y)dy \tag{A10}$$

$$M_5 = M_D l_1 f(l_1) + \int_0^L \rho S y f(y)dy$$

$$k = E\int_0^L I_m h^2(y)dy$$

$$k_a = E\int_0^L I_a h^2(y)dy \tag{A11}$$

Appendix B: Parametric Equations in Case of an Imposed Rotation

In the case of a sinusoidal imposed rotation of the base $\dot{\alpha}_s = a\omega\cos(\omega t)$, Eqs. (A3)–(A11) are modified and lead to new components, thus, Eq. (A2) becomes

$$\begin{aligned} m\ddot{q}_1 - \Omega I_{y2}\dot{q}_2 + [k + a^2\omega^2(I_{m2} - I_{y2})\cos^2(\omega t)]q_1 \\ = I_{y1}a\Omega\omega\cos(\omega t) + M_u\sin(\omega t) \\ m\ddot{q}_2 + \Omega I_{y2}\dot{q}_1 + [k - a^2\omega^2 M_2\cos^2(\omega t)]q_2 \\ = (M_5 + I_{m1})a\omega^2\sin(\omega t) + M_u\cos(\omega t) \end{aligned} \tag{B1}$$

where $m_{11}=m_{22}=m$ and $m_{12}=m_{21}=0$. Thus, parametric terms such as $q_i\cos^2(\omega t)$ are included in the system of equations. Equations (B1) can be rewritten as

$$\begin{aligned} m\ddot{q}_1 - \Omega I_{y2}\dot{q}_2 + kq_1 = \omega^2 A\cos^2(\omega t)q_1 + \Omega\omega B\cos(\omega t) + M_u\sin(\omega t) \\ m\ddot{q}_2 + \Omega I_{y2}\dot{q}_1 + kq_2 = \omega^2 C\cos^2(\omega t)q_2 + \omega^2 D\sin(\omega t) + M_u\cos(\omega t) \end{aligned} \tag{B2}$$

where the following substitutions have been made:

$$A = a^2(I_{y2} - I_{m2}); \quad B = I_{y1}a; \quad C = a^2M^2; \quad D = a(M_5 + I_{m1}) \tag{B3}$$

Then the equations are ordered by using a small bookkeeping parameter ε [13]. In our case, only the terms depending on the support motion are concerned.

$$\begin{aligned} m\ddot{q}_1 - \Omega I_{y2}\dot{q}_2 + kq_1 = \varepsilon\omega^2 A\cos^2(\omega t)q_1 + \varepsilon\Omega\omega B\cos(\omega t) \\ + M_u\sin(\omega t) \\ m\ddot{q}_2 + \Omega I_{y2}\dot{q}_1 + kq_2 = \varepsilon\omega^2 C\cos^2(\omega t)q_2 + \varepsilon\omega^2 D\sin(\omega t) \\ + M_u\cos(\omega t) \end{aligned} \tag{B4}$$

Now, the multiple scales method is applied up to the first order with

$$\begin{aligned} q_1(t,\varepsilon) = q_{10}(T_0,T_1,T_2,\dots) + \varepsilon q_{11}(T_0,T_1,T_2,\dots) + O(\varepsilon^2) \\ q_2(t,\varepsilon) = q_{20}(T_0,T_1,T_2,\dots) + \varepsilon q_{21}(T_0,T_1,T_2,\dots) + O(\varepsilon^2) \end{aligned} \tag{B5}$$

Substituting Eqs. (B5) into (B4) and equating coefficients of like power ε, this yields to a set of equations

$$\begin{aligned} mD_0^2 q_{10} - \Omega I_{y2}D_0 q_{20} + kq_{10} = M_u\sin(\omega t) \\ mD_0^2 q_{20} + \Omega I_{y2}D_0 q_{10} + kq_{20} = M_u\cos(\omega t) \end{aligned} \tag{B6}$$

and

$$\begin{aligned} mD_0^2 q_{11} - \Omega I_{y2}D_0 q_{21} + kq_{11} = -2mD_0D_1q_{10} + \Omega I_{y2}D_1 q_{20} \\ + A\omega^2\cos^2(\omega t)q_{10} + B\omega\Omega\cos(\omega t) \\ mD_0^2 q_{21} + \Omega I_{y2}D_0 q_{11} + kq_{21} = -2mD_0D_1q_{20} - \Omega I_{y2}D_1 q_{10} \\ + C\omega^2\cos^2(\omega t)q_{20} + D\omega^2\sin(\omega t) \end{aligned} \tag{B7}$$

A study of (B7) shows that interesting resonant terms are obtained for

$$\begin{aligned} 2\omega - \omega_1 \approx \omega_1 \quad \text{or} \quad \omega \approx \omega_1 \\ 2\omega - \omega_1 \approx \omega_2 \quad \text{and} \quad (2\omega - \omega_2 \approx \omega_1) \quad \text{or} \quad \omega \approx \frac{(\omega_1 + \omega_2)}{2} \\ 2\omega - \omega_2 \approx \omega_2 \quad \text{or} \quad \omega \approx \omega_2 \\ 2\omega + \omega_1 \approx \omega_2 \quad \text{or} \quad \omega \approx \frac{(\omega_2 - \omega_1)}{2} \end{aligned} \tag{B8}$$

where ω_1 and ω_2 are the natural frequencies of the rotor (corresponding to backward and forward modes), which are explicitly depending on Ω [1].

References

[1] Lalanne, M., and Ferraris, G., 1998, *Rotordynamics Prediction in Engineering*, 2nd ed., Wiley, New York.

[2] Subbiah, R., Bhat, R., and Sankar, T. S., 1985, "Response of Rotors Subjected to Random Support Excitations," Trans. ASME, J. Vib., Acoust., Stress, Reliab. Des., **107**, pp. 453–459.

[3] Berlioz, A., and Ferraris, G., 1986, "Utilisation de la Sous-Structuration en Dynamique des Rotors," Méc. Mat. Elec., **416**, pp. 30–33.

[4] Suarez, L. E., Rohanimanesh, M. S., and Singh, M. P., 1992, "Seismic Response of Rotating Machines," Earthquake Eng. Struct. Dyn., **21**, pp. 21–36.

[5] Beley-Sayettat, A., 1994, "Effet des Dissymétries et Effet Sismique en Dynamique des Rotors," Ph.D. thesis No. 94-0105, INSA-Lyon, France.

[6] Ganesan, R., and Sankar, T. S., 1993, "Resonant Oscillations and Stability of Asymmetric Rotors," ASME Design Technical Conference, 14th Biennial Conference on Mechanical Vibration and Noise, Alburquerque, NM, Vol. 56, pp. 131–137.

[7] Ganesan, R., and Sankar, T. S., 1993, "Non-Stationary Vibrations of Rotor Systems With Non-Symmetric Clearance," ASME Design Technical Conference, 14th Biennial Conference on Mechanical Vibration and Noise, Alburquerque, NM, Vol. 56, pp. 295–301.

[8] Kang, K., Chang, Y-P., Tsai, J-W., Mu, L-H., and Chank, Y-F., 2000, "An Investigation in Stiffness Effects on Dynamics of Rotor-Bearing-Foundation Systems," J. Sound Vib., **231**(2), pp. 343–374.

[9] Edwards, S., Lees, A. W., and Friswell, M. I., 2000, "Experimental Identification of Excitation and Support Parameters of a Flexible Rotor-Bearings-Foundation System From a Single Run-Down," J. Sound Vib., **232**(5), pp. 963–992.

[10] Bonello, P., and Brennan, M. J., 2001, "Modeling the Dynamical Behavior of a Supercritical Rotor on a Flexible Foundation Using the Mechanical Impedance Technique," J. Sound Vib., **239**(3), pp. 445–466.

[11] Duchemin, M., Berlioz, A., and Ferraris, G., 2001, "Modélisation du Comportement Dynamique des Rotors Embarqués," *Proc. of XVème Congrès Français de Mécanique*, 15éme Congrés Français de Mécanique, Nancy, France, on CD ROM.

[12] Duchemin, M., Ferraris, G., and Berlioz, A., 2006, "Behavior and Stability of a Rotor Under Base Excitation," ASME J. Vibr. Acoust., in press.

[13] Nayfeh, A. H., 1993, *Method of Normal Form*, Wiley, New York.

[14] Bolotin, V. V., 1964, *The Dynamic Stability of Elastic Systems*, Translated from Russian, Holden Day, Inc., San Francisco.

Accepted Manuscript